

Image-derived MTF method and MTF compensation for CBERS-02B WFI imager

LI Xiao-ying^{1,2}, GU Xing-fa^{1,2}, YU Tao^{1,2}, CHENG Tian-hai^{1,2}, GAO Hai-liang^{1,2},
LI Jia-guo^{1,2}, YANG Xiao-feng^{1,2}

1. State Key Laboratory of Remote Sensing Science, Jointly Sponsored by the Institute of Remote Sensing Applications of Chinese Academy of Sciences and Beijing Normal University, Beijing 100101, China;

2. Demonstration Centre for Spaceborne Remote Sensing National Space Administration, Beijing 100101, China

Abstract: In this paper, a method to evaluate the in-flight MTF (Modulate Transfer Function) of the WFI (Wide Field Imager) on CBERS-02B is presented and the WFI images are restored. The CCD is another payload on CBERS-02B with high spatial resolution. Using the CCD images as high resolution images, the two-image comparison approach is applied to determine the MTF of the WFI with a pair of images acquired over Beijing on Nov. 10, 2007. As the results, MTF values in three directions are derived. The MTF values at Nyquist frequency in cross-track, in-track and 45° directions were respectively about 0.43, 0.52 and 0.35 for red band and 0.30, 0.46 and 0.36 for near-infrared band. Image-derived MTF values are applied to calculate the half bandwidths of the WFI. The results indicate that the instant fields of view of the WFI in the cross-track, in-track and 45°-track directions were respectively 1.188 pixels, 1.165 pixels and 1.281 pixels for red band, and respectively 1.258 pixels, 1.195 pixels and 1.326 pixels for near-infrared band. Weiner filter model is used to perform the MTF compensation for WFI images. The results show that the restored image seemed clearer and contained more detailed information.

Key words: CBERS-02B, CCD, MTF, the two-image comparison approach

CLC number: TP702 **Document code:** A

1 INTRODUCTION

The MTF is a fundamental imaging system design specification and system quality metric often used in remote sensing. The MTF is acquired by performing FFT (fast fourier transform) on PSF (point spread function) and normalizing its modulation. It results from the cumulative effects of the instrumental optics (diffraction, aberrations, focusing error), integration on a photosensitive surface, charge diffusion along the array and image motion induced by the movement of the satellite during imaging (Leger *et al.*, 2003). The MTF can be tested accurately in the lab, but it will change due to the refocus of the sensor and the MTF of the atmosphere. Thus, in-flight MTF determining and compensation is a vital step for the comprehensive applications of WFI images.

Many approaches have been proposed to perform in-flight MTF measurement. The impulse method was often used in lab to measure the PSF (Du & Voss, 2004). The MTF of HRG on SPOT 5 was obtained by directing a lamp to satellite (Leger *et al.*, 2003). The most common method was to use line-feature or edge-feature images. Edge-feature method required that the

edge had a high fidelity representation of the ESF (edge spread function), which had been successfully applied to many sensors (Forster & Best 1994; Kohm, 2004; Taeyoung, 2002). Different techniques were presented according to the width of lines. Schowengerdt *et al.* (1985) took a linear bridge as an ideal pulse to determine the MTF for Landsat 5-TM, since the width of the bridge was less than one pixel, which was the LSF (line spread function) itself. For lines having several pixels width, left and right LSF could be determined by two edge method (Forster & Best 1994). When monitoring the MTF for IKONOS by imaging linear designed tarps, Taeyoung(2002) applied the pulse method. In general, these measurement techniques required that the targets had a particular size and orientation. The method of two-image comparison was proposed by Schowengerdt and had been used widely (Schowengerdt *et al.*, 1985; Bretschneider *et al.*, 2001; Viallefont-Robinet & Henry, 2000). This approach has no special requirements for the scenes except that they should contain a variety of features, so it is suitable for low ground spatial resolution sensors.

Some studies have been done focusing on the sensors of CBERS series satellites. Liu *et al.* (2004) used line-feature image to calculate the PSF of the CCD on CBERS-01. Gu *et al.*

Received date: 2008-04-11; **Accepted date:** 2008-08-25

Foundation: Project 40701109 supported by National Science Foundation; Project 2006AA12Z113 supported by The National High Technology Research and Development Program of China; Supported by the Knowledge Innovation Program of the Chinese Academy of Science and State Key Laboratory of Remote Sensing Science, Institute of Remote Sensing Applications of Chinese Academy of Sciences (08S00700CX)

First author biography: LI Xiao-ying (1975—), female, Associate Professor. Get Ph.D in the institute of remote sensing applications, CAS in 2006. Research interest is radiometric calibration, sensor and atmosphere MTF measurement and compensation. Currently, 11 representative papers haven been published, including 4 papers in SCI.

(2005) and Li (2006) proposed a new technique to perform in-flight MTF measurement for the CCD on CBERS-02. Li *et al.* (2009) compared two techniques of two-image comparison approach. This study is based on the result of Li *et al.*'s research (2009), and it uses the same technique to perform the MTF measurement for WFI on CBERS-02B and makes the MTF compensation for WFI images using the image-derived MTF.

2 TWO-IMAGE COMPARISON APPROACH

This approach suggested that the observed images were the convolution between the real scene and the point spread function (PSF) of the imaging system, as shown in Equ.(1) (Schowengerdt *et al.*, 1985).

$$i(x, y) = o(x, y) * p(x, y), \quad (1)$$

where, $i(x, y)$ is the observed image; $o(x, y)$ is the real scene; $p(x, y)$ is the PSF of imaging system; x and y are the spatial coordinates of the image. When transformed to frequency domain, the formula changes to be Equ. (2).

$$I(u, v) = O(u, v) \times F(u, v), \quad (2)$$

where, $I(u, v)$, $O(u, v)$ and $F(u, v)$ are the FFT of $i(x, y)$, $o(x, y)$ and $p(x, y)$ respectively; u and v are the frequency coordinates of the x and y . Comparing with low spatial resolution image, the high spatial resolution image can be regarded as the real scene in Equ. (1).

There are two different techniques for the two-image comparison approach. One technique used by Viallefont-Robinet and Henry (2000) performed the FFT on the low and high ground spatial resolution images and picked out the common frequencies. Then the ratio of their modulations was determined. The other technique was proposed by Schowengerdt *et al.* (1985). This technique was required to magnify the low spatial resolution image and made the accurate geometrical registration of the magnified image and high resolution image. Then, the common research area was selected to achieve the ratio of the

FFT of the two images. The research of Li *et al.* (2009) showed that results of two techniques were somewhat different, though they should be consistent theoretically. This difference could be due to the complicated preprocessing in the technique used by Schowengerdt. Therefore, this study applied the technique used by Viallefont-Robinet and Henry to derive the MTF of WFI.

3 IMAGE SELECTION AND PREPROCESSING

The spatial resolution of WFI on CBERS-02B is 258m, while the CCD is 19.5m. They are about 13 times different. The CCD and WFI view the scene at the same time. Thus, the change of the atmosphere condition can be neglected. The CCD's band 3 and 4 correspond to WFI's red band and near-infrared band respectively. Currently, the spectral band response functions of WFI on CBERS-02B are unavailable. The WFI sensor carried on CBERS-02B is similar with that on CBERS-02. Therefore the spectral band response function of the WFI on CBERS-02 were used to compare with the response functions of CCD on CBERS-02B. The spectral band response functions of two corresponding spectral bands of CCD and WFI were similar, which were shown in Fig.1 and Table 1. The ranges of their wave bands were consistent, with 15nm difference of the centre wavelength of red band and 11nm difference of the near-infrared band.

The information of the image pair used to determine the in-flight MTF of WFI was listed in Table 2.

The sub-images were extracted from this pair of images. The size of the sub-image of WFI image scene was about 231×231 pixels, and that of CCD image scene was about 3001×3001 pixels. The selected area was Beijing city and the outskirt, which mainly covered river, sea, cities, and highways, etc. The selected site was near nadir viewed and had little relief to diminish the effect of the landform and its shadow. The study area of red band of CCD and WFI was shown in Fig. 2.

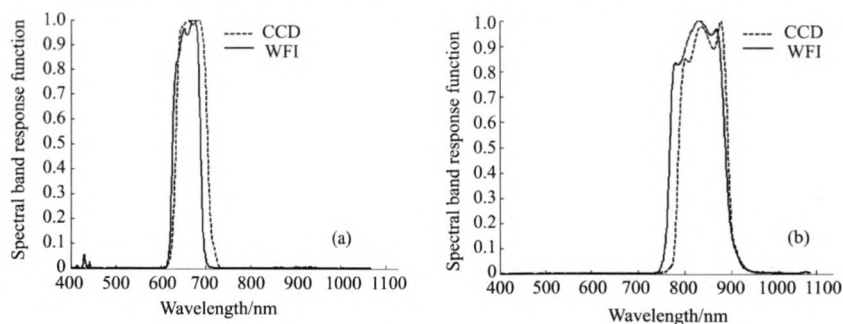


Fig. 1 The spectral band response functions of CCD and WFI
(a) Red band; (b) Near-infrared band

Table 1 The red and near-infrared bands of CCD and WFI

CCD bands	CCD/nm	Centre wavelength/nm	Spatial resolution /m	WFI bands	WFI /nm	Centre wavelength /nm	Spatial resolution /m
3	630—690	671.96	19.5	1	630—690	657.74	258
4	770—890	843.1	19.5	2	770—890	831.98	258

Table 2 The information of studied images of CCD and WFI

	Acquisition time	Path/Row	Center coordinate	Viewing geometries/(°)
WFI	2007-11-10 03:13:36.000	1/53	117.228838E/ 47.031887N	-15.107908 /170.067744
CCD	2007-11-10 03:14:10.000	1/55	40.499452E/ 116.715493N	0/170.067744

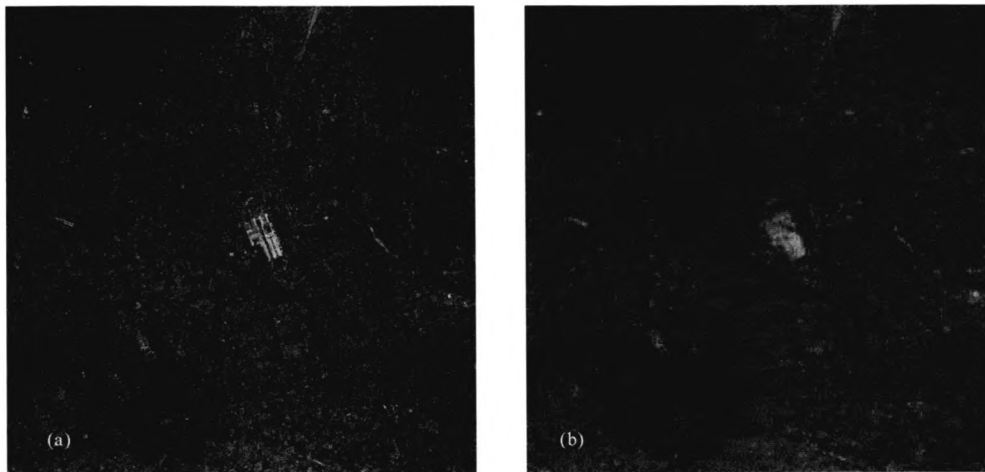


Fig. 2 Red band of studied image
(a) CCD; (b) WFI

4 RESULTS OF MTF MEASUREMENT FOR WFI

The images used in this study were level 1 products, which means that they had not been geometrically corrected. And no processing was applied to these images. Based on the technique used by Viallefont-Robinet and Henry (2000) and Li *et al.* (2008), the sub-image pair of the selected study area was used to determine the in-flight MTF of WFI. Before performing FFT, a hanning window was applied to both of CCD and WFI sub-images to diminish the aliasing at high frequencies. Then, the FFT could be applied to the windowed CCD and WFI sub-images and shift the 0 frequency to the center. The modulations of the FFT of CCD and WFI sub-images were normalized. The Fig. 3 (a) and Fig. 3 (b) were respectively the logarithm of modulations for CCD and WFI sub-images.

The modulations of common frequencies of the WFI and CCD sub-images were extracted (Li, 2006) and the ratio of the modulations was calculated to get a ratio matrix. Then the following processes were applied to the ratio matrix to achieve the smooth MTF curves. First, a median filtering was applied to smooth the noise of the ratio matrix. Second, a threshold 1.5 was used to delete the values which were larger than the threshold in the smoothed ratio matrix. Third, in the matrix, values belonging to the same ring and to the range of $[-15^\circ, +15^\circ]$ were averaged as the cross-track MTF; values belonging to $[+75^\circ, +105^\circ]$ were taken as in-track MTF; while those belonging to $[+30^\circ, +60^\circ]$ were regarded as the 45° axis. More details could be found in references (Schowengerdt *et al.*, 1985; Viallefont-Robinet & Henry, 2000). Forth, the interpolating process was needed to avoid the aliasing at high frequencies. Finally, a four-term polynomial was applied to get a smooth MTF curve. The MTF curves of red and near-infrared band of WFI in three directions were shown in Fig. 4 and Fig. 5. Only the MTF values from the frequency 0 to 0.5 were calculated, since those from the frequency -0.5 to 0 could be determined according to the symmetry of the modulations.

On Fig. 4 and Fig. 5, the MTF values at Nyquist frequency of

red band for WFI were 0.43, 0.52 and 0.35 in cross-track, in-track and 45° directions respectively, and 0.3, 0.46 and 0.36 for near-infrared band in three directions respectively. MTF values of both bands at different frequencies in three directions were listed in Table 3. For both bands, the MTF values in in-track direction were higher than those in cross-track and 45° directions and the attenuation rate of MTF values from low to high frequency showed slower in in-track direction. For red band, from 0.1 to 0.2, 0.2 to 0.3, 0.3 to 0.4 and 0.4 to 0.5 frequencies, the attenuation rates of MTF values were 10.84%, 13.71%, 16.01% and 7.68% respectively in in-track direction, 14.59%, 8.96%, 14.91% and -6.08% respectively in cross-track direction and 29.29%, 18.62%, 4.9% and 6.9% respectively in 45° direction. The attenuation rates of MTF values at frequency of about 0.2 would affect the bandwidth directly. The comparison among the three directions was similar for near-infrared band.

The LSF could be calculated by reversing three directional MTFs. The half bandwidths, that was the effective instant field of view, could be determined from LSF. Results were shown in Fig. 6. The half bandwidths of red band of WFI were 1.188 pixels, 1.165 pixels and 1.281 pixels in cross-track, in-track and 45° directions, which were 306.5m, 300.5m and 330.5m. For near-infrared band, they were 1.258 pixels, 1.195 pixels and 1.326 pixels, which were 324.5m, 308.3m and 342.1m.

5 MTF COMPENSATION FOR WFI IMAGES

The image-derived MTF in this study was applied to perform the MTF compensation for WFI images. The MTF values determined were one-dimension. To restore images based on MTF compensation, the two-dimension MTF was required. Two-dimension MTF model used in the references (Gu *et al.*, 2005; Li, 2006) was adopted in this study and weiner filter model was chosen to perform the MTF compensation for WFI images.

Weiner filter model was widely used in restoring images (Fonseca *et al.*, 1993; Li, 2006; Liu *et al.*, 2004). It could be

applied in frequency domain, as shown in Equ. (3) and (4).

$$P(u,v) = \frac{1}{M(u,v)} \times \left\{ \frac{[M(u,v)]^2}{[M(u,v)]^2 + k} \right\}, \quad (3)$$

$$R(u,v) = I(u,v) \times P(u,v), \quad (4)$$

where, $P(u,v)$ was the Wiener filter; k was relative to Signal-to-Noise (SNR) of the image, which was often substituted by a constant; $R(u,v)$ was the frequency spectrum of the restored image; $I(u,v)$ was the frequency spectrum of the original image; and $M(u,v)$ was the two dimensional MTF.

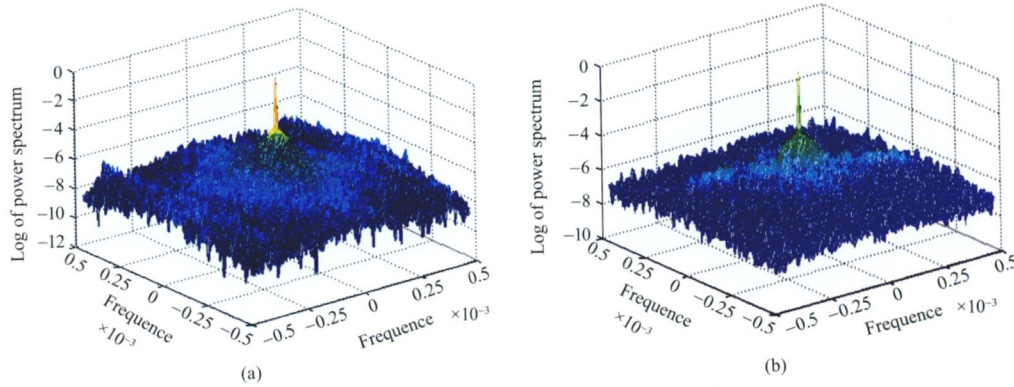


Fig. 3 Log of modulate of FFT for CCD and WFI images (a) WFI; (b) CCD

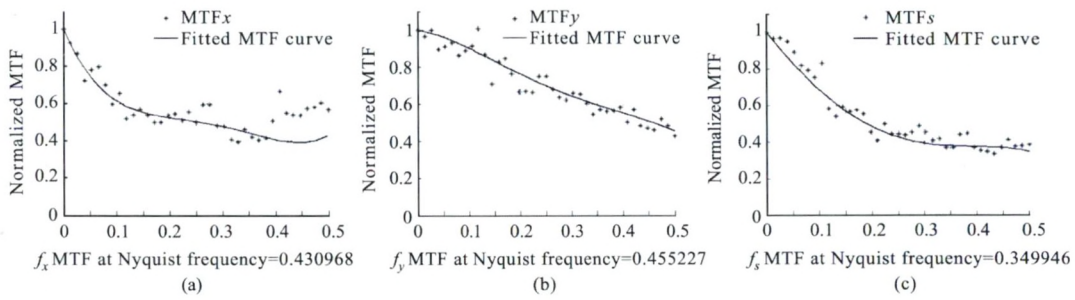


Fig. 4 MTF of red band of WFI in three directions (a) Cross-track MTF; (b) In-track MTF; (c) 45° direction MTF

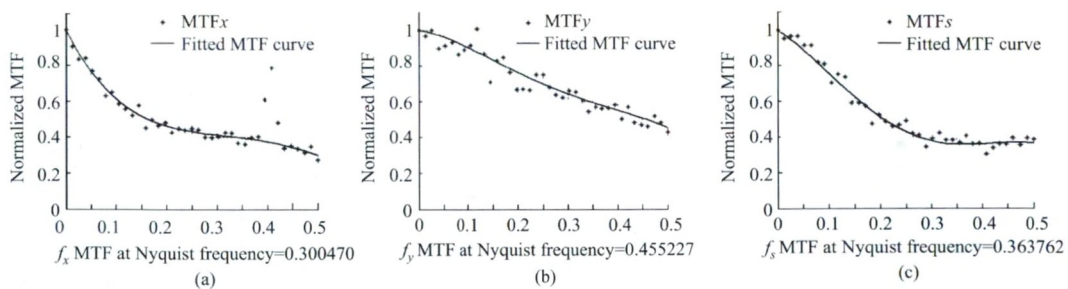


Fig. 5 MTF of near-infrared band of WFI in three directions (a) Cross-track MTF; (b) In-track MTF; (c) 45° direction MTF

Table 3 MTF values of red and near-infrared bands of WFI in three directions

		0.1 frequency	0.2 frequency	0.3 frequency	0.4 frequency	0.5 frequency
Red band	MTF in cross-track direction	0.6141	0.5245	0.4775	0.4063	0.4310
	MTF in in-track direction	0.8746	0.7798	0.6729	0.5652	0.5218
	MTF in 45° direction	0.6865	0.4854	0.3950	0.3757	0.3499
Near-infrared band	MTF in cross-track direction	0.6145	0.4621	0.4127	0.3758	0.3005
	MTF in in-track direction	0.9019	0.7639	0.6437	0.5525	0.4552
	MTF in 45° direction	0.7549	0.5120	0.3783	0.3602	0.3638

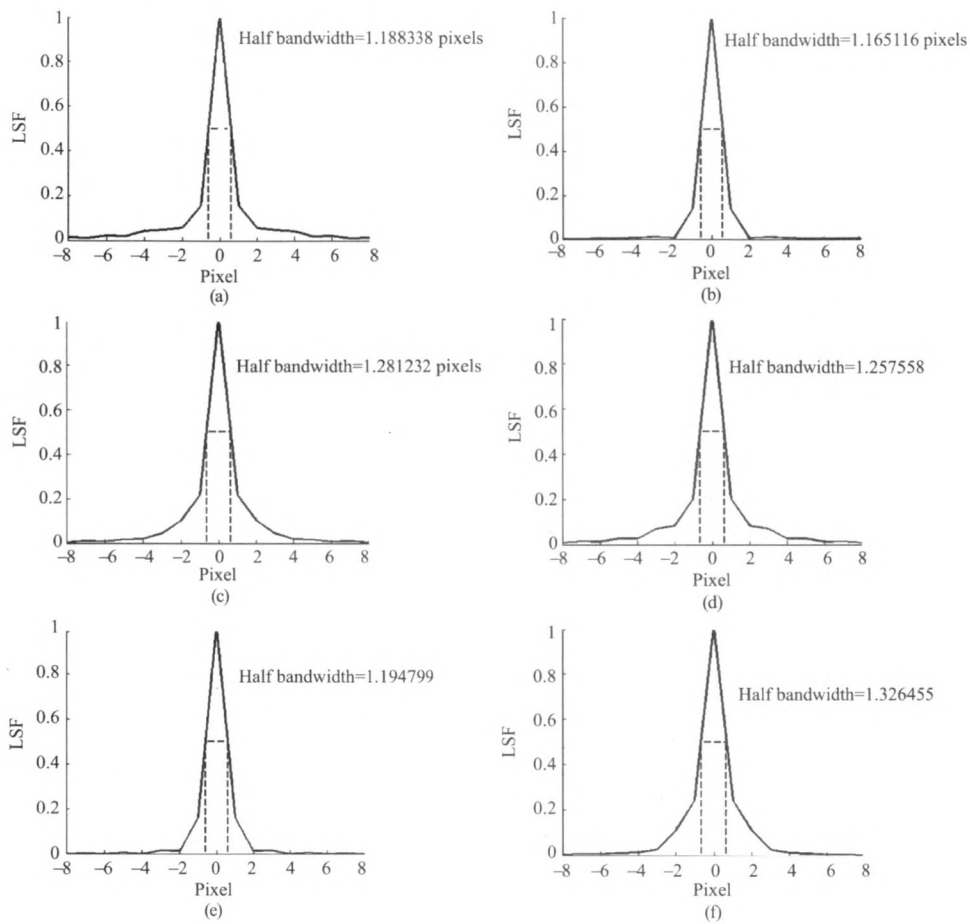


Fig. 6 The PSF for two bands of WFI in three directions.
 (a) Cross-track of red band; (b) In-track of red band; (c) 45° direction of red band; (d) Cross-track of near-infrared band;
 (e) In-track of near-infrared band; (f) 45° direction of near-infrared band

The MTF compensation was performed for WFI image acquired in 1st path, 53rd row on Nov. 10, 2007. The sub-images of original and compensated images in red and near-infrared bands were shown in Fig. 7 and Fig. 8. Comparing the images before and after compensation, the compensated images became clearer and contained more details than the original ones. For example, in the window marked with the white frame in Fig. 7 and Fig. 8, the texture of the lattice ponds of aquaculture near the coast became clearer in the compensated images than that in the original images. It is much clearer in the magnified images inside the white-border rectangle. It could also be found that the contrast between different features was more evident in the compensated images of both two bands. Fig. 7 and Fig. 8 also showed that the outlines of rivers in the compensated images appeared clearer.

However, the MTF compensation would magnify the noise of the original images. It can be observed from the magnified images inside the white-border rectangle in Fig. 7 and Fig. 8, that the original images were more smoother, while the compensated images contained some noise in the high frequencies brought in by MTF compensation processing. Currently, it is a hard and hot topic for researchers about how to restrain noise in the MTF compensation processing.

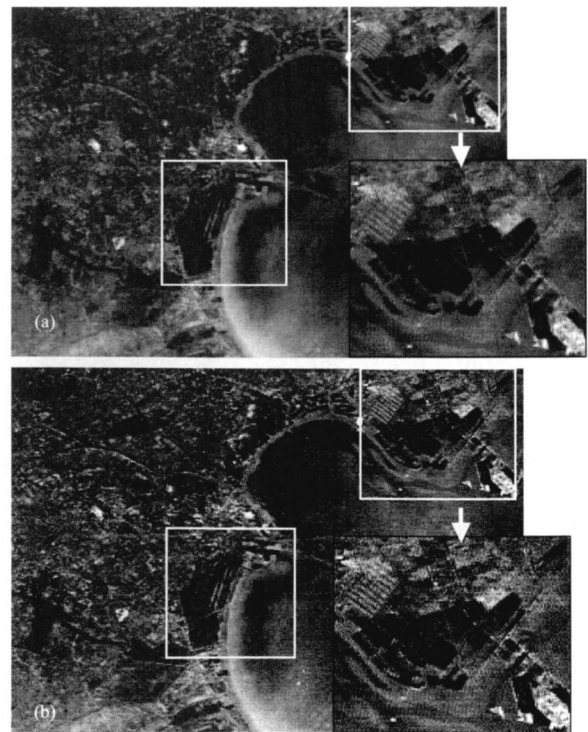


Fig. 7 MTF compensation for red band of 1/53 WFI image on 2007-11-10.
 (a) Original image; (b) Restored image

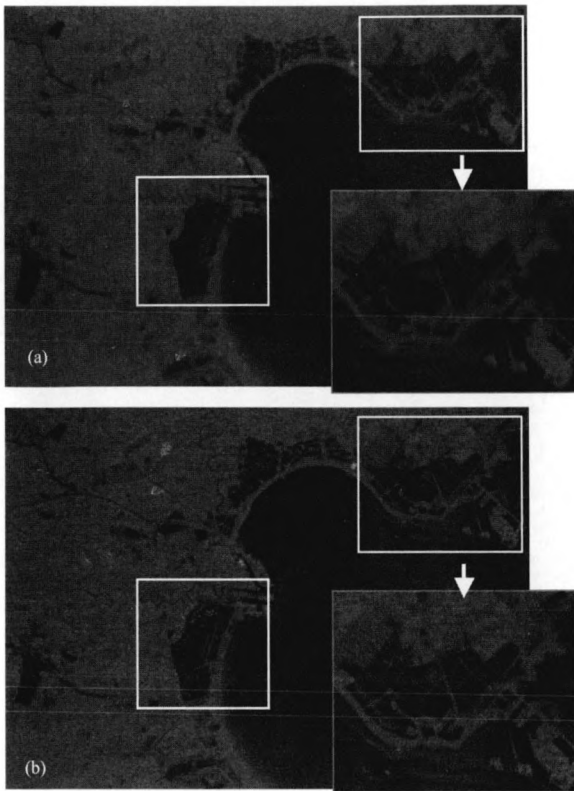


Fig. 8 MTF compensation for near-infrared band of 1/53 WFI image on 2007-11-10.
(a) Original image; (b) Restored image

6 CONCLUSION AND DISCUSSION

Based on the high spatial resolution images of the CCD, this study used the two-image comparison approach to determine the MTF of the WFI. The image-derived MTF curves and half bandwidths in three directions were achieved. The half bandwidths in cross-track, in-track, 45° directions were 1.188 pixels, 1.165 pixels and 1.281 pixels respectively for red band, and 1.258 pixels, 1.195 pixels and 1.326 pixels respectively for near-infrared band. Then, the image-derived MTF curves were applied to perform MTF compensation for WFI images. The research results demonstrated that the two-image comparison approach is suitable for low spatial resolution sensors, like WFI, and that the MTF compensation will bring more rich and detailed information than the original images.

However, further researches should be undertaken. The two-image comparison approach has some uncertainties, because the MTF measurement results were directly relative to the quality of the high spatial resolution images, which is difficult to quantify. And MTF measurement results will be different using different image pair of scenes. In this study, only one image pair of scene was used to evaluate the MTF of WFI. Further study should be carried out to validate and analyze the influence. On the other hand, the compensated WFI images showed more noise in the high frequencies because the MTF compensation processing is possible to magnify noise. There-

fore, the further research on the MTF compensation model should focus on reducing noise when performing MTF compensation.

Acknowledgements: The CCD and WFI images were kindly offered by China Centre for Resource Satellite Data & Application.

REFERENCES

- Bretschneider T, Bones P J, McNeill S and Pairman D. 2001. Image-based quality assessment of SPOT data. Proceedings of the American Society for Photogrammetry & Remote Sensing, St. Louis, April, 2001
- Du H and Voss K J. Effects of point-spread function on calibration and radiometric accuracy of CCD camera. *Applied Optics*, **43** (3): 665—670
- Fonseca L M G, Prasad G S S D and Mascarenhas N D A. 1993. Combined interpolation—restoration of Landsat images through FIR filter design techniques. *International Journal of Remote Sensing*, **14** (13): 2547—2561
- Forster B C and Best P. 1994. Estimation of SPOT P-mode point spread function and derivation of a deconvolution filter. *ISPRS Journal for RS and GIS*, **49** (6): 32—42
- Gu X F, Li X Y, Min X J, Yu T, Sun J J, Zeng Y, Xu H and Guo D. 2005. In flight MTF monitoring and compensation for CCD camera on CBERS-02. *Science in China Series E-Engineering & Materials Science*, **48** (Suppl.1): 29—43
- Kohm K. 2004. Modulation transfer function measurement method and results for the orbview-3 high resolution imaging satellite. Proceedings of ISPRS 2004, Istanbul, Turkey, July 12—23
- Leger D, Viallefont F, Hillairet E and Meygret A. 2003. In-flight refocusing and refocusing and MTF assessment of SPOT5 HRG and HRS. *SPIE*, **4881**: 224—231
- Li X Y. 2006. In Flight Radiometric Calibration and Pixel Based Calibration for CCD Camera and WFI Imager on CBERS-02. Ph.D dissertation of the Institute of Remote Sensing Applications, CAS
- Li X Y, Gu X F and Yu T. 2009. In-flight MTF measurement and compensation for CBERS-02 WFI imager. *International Journal of Remote Sensing*, **30**(4): 829—839
- Liu Z J, Wang C Y and Luo C F. 2004. Estimation of CBERS-21 Point Spread Function and Image Restoration. *Journal of Remote Sensing*, **8** (3): 234—238
- Schowengerdt R A, Archwamety C and Wrigley R C. 1985. Landsat thematic mapper image-derived MTF. *Photogrammetric Engineering and Remote Sensing*, **51** (9): 1395—1406
- Taeyoung Choi. 2002. IKONOS Satellite on Orbit Modulation Transfer Function (MTF) Measurement Using Edge and Pulse Method. A thesis Submitted in Partial Fulfillment of the Requirements for the Master of Science Major in Engineering South Dakota State University
- Viallefont-Robinet F and Henry P. 2000. VEGETATION MTF in-flight measurement using HRVIR. Proceeding of the SPIE-Earth Observing Systems V, **4135**: 314—323

CBERS-02B 卫星 WFI 成像在轨 MTF 估算 与图像 MTF 补偿

李小英^{1,2}, 顾行发^{1,2}, 余 涛^{1,2}, 程天海^{1,2},
高海亮^{1,2}, 李家国^{1,2}, 杨晓峰^{1,2}

1. 遥感科学国家重点实验室, 中国科学院 遥感应用研究所、北京师范大学, 北京 100101;

2. 国家航天局 航天遥感论证中心, 北京 100101

摘 要: 基于高分辨率图像对比法, 利用同一卫星平台上空间分辨率 19.5m 的 CCD 相机图像对 CBERS-02B 卫星上空间分辨率为 258m 的 WFI 成像仪图像进行在轨 MTF(modulate transfer function)测量, 获得 WFI(wide field imager)相机沿轨、跨轨与 45°方向的 MTF 曲线, 并计算出 3 个方向的线扩展函数 LSF(line spread function), 获得 3 个方向的有效半带宽。结果表明 WFI 相机红波段跨轨、沿轨与 45°方向的有效半带宽, 即有效瞬时视场, 分别为 1.188, 1.165 与 1.281 个像元, 近红外波段为 1.258, 1.195 与 1.326 个像元。基于获得的 MTF, 利用维纳滤波法对 WFI 图像进行补偿, 部分恢复了 WFI 图像的细部信息。

关键词: CBERS-02B, CCD, MTF, 高分辨率图像对比法

中图分类号: TP702

文献标识码: A

1 引 言

摄影系统在进行影像获取时会产生亮度的模糊, 对产生模糊的描述表示为调制解调函数(modulate transfer function, MTF)。点扩散函数(point spread function, PSF)傅里叶变换后, 对模进行归一化就是 MTF。MTF 是影像系统的图像质量特性之一, 它是由仪器光学特性(折射、杂散光、聚焦错误)、感光表面的积分、沿着阵列的电荷漫射以及摄影时卫星的运动使图像振动等综合因素造成的(Leger 等, 2003)。发射前, 传感器的 MTF 在实验室精确测量, 由于发射过程中的振动及从空气中进入真空的变化会使传感器重新聚焦, 另外受大气 MTF 的影响, 使它的 MTF 发生衰减。MTF 的在轨测量以及图像 MTF 补偿是保证遥感图像质量的重要环节。

目前, 按测量目标分, 常用的 MTF 在轨测量方法有: 高分辨率图像对比法、点源法、边缘地物法及线性地物测量法。点源法是一种直接测量

PSF 的方法, 它是实验室内常用的方法(Du & Voss, 2004), 通过计算输入的点源脉冲来计算系统的 MTF。该方法也曾用于 SPOT5 上 HRG 的 MTF 在轨测量(Leger 等, 2003), 但在轨测量噪声影响很大。边缘地物法是一种间接测量 PSF 的方法, 已成功的用于 SPOT P-mode, OrbView-3, IKONOS 的在轨 MTF 测量(Forster & Best, 1994; Kohm, 2004; Taeyoung, 2002)。边缘地物法要求所选的边缘必须在主平面附近沿轨或垂直于轨道方向分布, 且与主平面有很小的夹角, 另外要求边缘有足够的长度。线状地物测量法也是一种间接测量 PSF 的方法, 在实际应用中, 根据线状地物的宽度而选择合适的方法。Schowengerdt 测量 Landsat5 TM 的 MTF 时, 用于测量 MTF 的桥面宽度小于 TM 图像的一个像元, 认为它是一个理想的线性脉冲响应, 以桥面图像本身作为线扩展函数(line spread function, LSF)(Schowengerdt 等, 1985)。SPOT 上的传感器进行 MTF 在轨测量时选择了各种宽度的线性地物, 对于宽的线性地物采用双边缘法, 分别得到线性地物的

收稿日期: 2008-04-11; 修订日期: 2008-08-25

基金项目: 国家自然科学基金资助项目(编号: 40701109), 863 计划资助项目(编号: 2006AA12Z113), 中国科学院知识创新工程青年人才领域前沿项目专项项目资助(编号: 08S00700CX)。

第一作者简介: 李小英(1975—), 女, 2006 年毕业于中国科学院遥感应用研究所, 获理学博士学位。主要研究方向为可见光/近红外传感器辐射特性校正与大气校正。发表论文 11 篇。E-mail: lixiaoying@irsa.ac.cn。

左右 LSF(Forster & Best, 1994)。Taeyoung 对 IKONOS 进行 MTF 评价时, 不仅利用各种自然景物还铺设了靶标, 将图像上得到的响应作为脉冲响应的输出, 根据靶标的宽度设计 Sine 脉冲输入, 输出与输入的比值即为系统的 LSF (Taeyoung, 2002)。线性地物法对测量目标具有较高的要求 (Forster & Best, 1994)。高分辨率图像法是 1978 年由 Schowengerdt 提出的。Schowengerdt 利用同步获取的航空相片, 测量 Landsat5 TM 的在轨 MTF (Schowengerdt 等, 1985)。SPOT 也曾选用 10m 的全色波段来测量多谱段的 MTF (Bretschneider 等, 2001), 以及采用 HRVIR 的图像作为高分辨率图像, 进行 VEGETATION 传感器 MTF 的在轨测量 (Viallefont-Robinet and Henry, 2000)。这种方法要求所获取的地表景物的信息要多样化, 不能太单一; 另外要求高、低分辨率两个传感器的波段设置较一致, 且获得的图像同步或准同步的。

针对 CBERS 卫星的传感器开展了相关研究。刘正军等(2004)利用线状地物计算 CBERS-01 卫星 CCD 的点扩散函数。Gu 等(2005)和李小英(2006)针对 CBERS 的 CCD 传感器提出模拟真实靶标场景法, 并结合现有的各种方法对 CCD 进行在轨 MTF 评价。Li 等(2009) 在分析比较两种高分辨率图像对比法的基础上, 对 CBERS-02 卫星的 WFI 成像仪进行在轨 MTF 测量与补偿。本文基于文献 Li 等(2009)的分析结果, 利用高分辨率图像对比法对 CBERS-02B 卫星的 WFI 相机进行在轨 MTF 测量, 并基于获得的 MTF 进行 WFI 图像 MTF 补偿。

2 高分辨率图像对比方法介绍

传感器所获取的图像是真实景物与传感器系统点扩散函数的卷积, 相对于低空间分辨率图像, 高空间分辨率图像可认为是真实景物, 将对应的高分辨率图像与低空间分辨率图像进行傅里叶变换, 可以在频率域确定出系统的 MTF。如公式(1)所示:

$$i(x, y) = o(x, y) * \text{PSF}(x, y) \quad (1)$$

式中, $i(x, y)$ 为低分辨率图像; $o(x, y)$ 为真实图像; $\text{PSF}(x, y)$ 为传感器的点扩散函数 PSF。将空间域的图像转换成频率域的频谱, 上式变为:

$$I(u, v) = O(u, v) \times \text{TF}(u, v) \quad (2)$$

式中, $I(u, v)$, $O(u, v)$ 及 $\text{TF}(u, v)$ 分别是 $i(x, y)$, $o(x, y)$ 及 $\text{PSF}(x, y)$ 的傅里叶变换形式。而 $\text{TF}(u, v)$ 的模即是所要的 MTF (Schowengerdt 等, 1985)。

高分辨率图像对比法有两种方法, 一种是

Viallefont-Robinet and Henry (2000)采用的提取共同频率法。这种方法只需将同一区域的高、低分辨率图像进行 FFT 变换, 截取它们的共同频率, 即可计算出低分辨率图像与高分辨率 FFT 模的比值。另一种方法是 Schowengerdt 等(1985)提出的方法, 该方法要求在预处理时将低分辨率图像放大成与高分辨率图像相似的比例, 进行比较精确的配准, 截取同样大小的区域, 得到两景图 FFT 变换后模的比值。文献 Li 等(2009)从原理与实际结果分析比较了这两种方法, 研究结果表明这两种方法从原理上结果是一致的, 但实际应用结果却有差异。研究分析进一步得出产生差异的原因可能是由于 Schowengerdt 的方法需要比较复杂的预处理及计算, 累积误差比较大引起的。因此本文基于文献 Li 等(2009)的分析结果, 采用 Françoise Viallefont-Robinet 的方法来进行 WFI 的 MTF 在轨测量。

3 图像选择及预处理

基于高分辨率图像对比法, 利用 CCD 相机图像作为高空间分辨率参考图像对 WFI 相机进行在轨 MTF 测量。CBERS-02B WFI 星下点空间分辨率为 258m, CCD 相机星下点空间分辨率为 19.5m, 两个传感器图像空间分辨率相差 13 倍左右。由于 CCD 相机与 WFI 在同一卫星平台 CBERS-02B 上, 对同一地区图像的获取基本上是同步的, 两景图像获取时的大气变化可以忽略。WFI 相机的第 1 波段与第 2 波段(红波段与近红外波段)与 CCD 相机的第 3、第 4 波段类似。目前还没从巴西得到 CBERS-02B WFI 的光谱响应函数, 以 CBERS-02 WFI 的光谱响应函数作为参考与 CBERS-02B CCD 相机的光谱响应函数进行比较。结果如表 1 与图 1。中心波长红波段相差在 15nm 以内, 近红外波段相差约 11nm。图 1 和图 2 显示, CCD 与 WFI 的光谱响应函数很相似, 利用 CCD 用于测量 WFI 的 MTF 是合理可行的。

用于 WFI 在轨 MTF 测量的图像信息如表 2。

分别从 CCD 与 WFI 图像上选取合适的研究区, 所选区域范围在 CCD 图像上大小为 3001 × 3001 像元, WFI 为 231 × 231 像元。所选择的区域是北京及周边地区, 主要包括城市、公路等地物。研究区域图像是近天顶观测且研究区的地形变化很小, 这些考虑将减小观测几何不同以及地形及其阴影所带来的影响。图 2 为所选研究区的 CCD 与 WFI 红外波段图像。

表 1 CCD 相机与 WFI 红波段与近红外波段

CCD 波段	CCD/nm	中心波长/nm	分辨率/m	WFI 波段	WFI/nm	中心波长/nm	分辨率/m
3	630—690	671.96	19.5	1	630—690	657.74	258
4	770—890	843.1	19.5	2	770—890	831.98	258

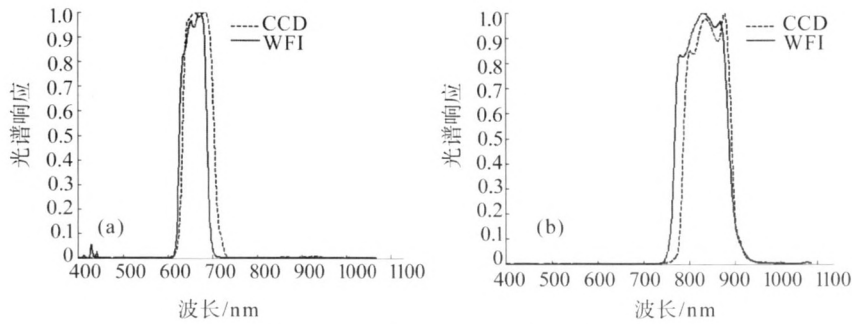


图 1 CCD 与 WFI 光谱响应函数

(a) 红波段; (b) 近红外波段

表 2 CCD 相机与 WFI 图像信息

	获取时间	Path/Row	图像中心经/纬度/(°)	观测天顶角/(°)/方位角/(°)
WFI	2007-11-10 03:13:36.000	1/53	117.228838/ 47.031887	-15.107908/170.067744
CCD	2007-11-10 03:14:10.000	1/55	40.499452/ 116.715493	0/170.067744

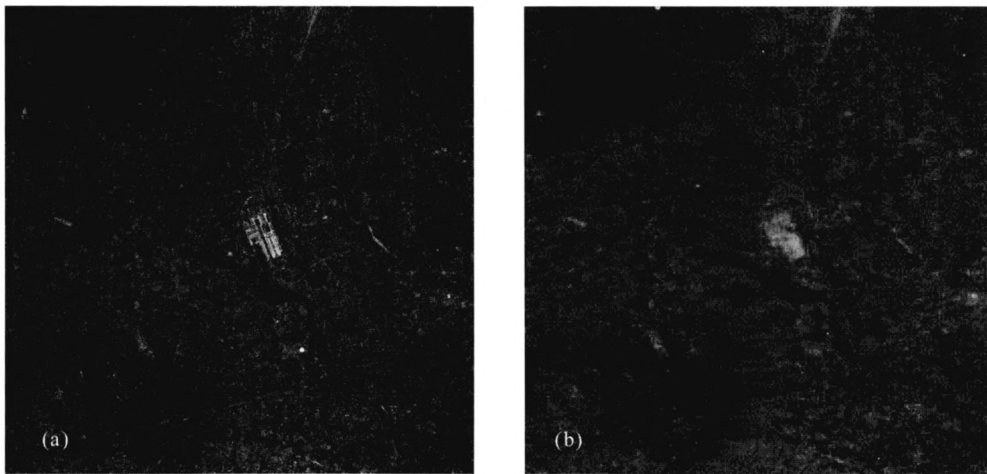


图 2 研究区图像红波段

(a) CCD; (b) WFI

4 WFI 成像仪的 MTF 测量结果

基于 Viallefont-Robinet & Henry (2000)测量 VEGETATION MTF 的方法, 利用研究区的 CCD 图像与 WFI 图像对进行 WFI 图像 MTF 测量。所用的 WFI 及 CCD 图像是只经过相对辐射校正的一级产品, 保持两个传感器原来的空间分辨率, 即 CCD 为 19.5m, WFI 为 258m。为了减小混叠现象, 在 FFT 变换前, 分别对研究区 CCD 与 WFI 图像进行 Hanning 窗滤波, 然后对 CCD 与 WFI 图像进行 FFT 变换后, 将 0 频率移到 FFT 频率图像中心并进行归

一化处理, 结果如图 3。图 3(a)与图 3(b)分别是 WFI 与 CCD 图像 FFT 变换后取对数的图像。

提取 WFI 和 CCD 共同频率的图像频谱(李小英, 2006)计算它们共同频谱的比值矩阵, 得到粗糙的初始二维 MTF。为了去除噪声, 采用 TM 和 VEGETATION 的高分辨率图像对比法对初始二维 MTF 的处理方法(Schowengerdt 等, 1985; Viallefont-Robinet and Henry, 2000): 首先对初始二维 MTF 进行 3×3 的中值滤波, 并设一个阈值 1.5, 去掉初始二维 MTF 矩阵中大于该阈值的元素, 得到较平滑的矩阵; 然后根据方位角平均求出跨轨方向[-15°, +15°]、

沿轨方向 $[+75^\circ, +105^\circ]$ 与 45° 斜方向 $[+30^\circ, +60^\circ]$ 3个方向各频率(文中所用频率为归一化频率)处的平均MTF值。由于模的对称性,只需求出 $0-0.5$ 频率处的MTF值,根据对称性即可得到 $-0.5-0$ 频率处的MTF值。WFI红波段与近红外波段在高频处频率混叠严重,MTF值在频率 0.38 以上噪音明显,取 $0-0.38$ 频率的值对 $0.3-0.5$ 频率的MTF值进行线性外延插值以避免频率混叠现象,修正后两个波段3个方向的MTF如图4与图5。

从图4和图5可以看出,在Nyquist频率处,红波段跨轨方向的MTF值约为 0.43 ;沿轨方向的MTF值约为 0.52 ; 45° 方向MTF值约为 0.35 ; 近红外波

段在上述3个方向分别为: $0.30, 0.46, 0.36$ 。表3列出了不同频率处的MTF值。可以看出无论是红波段还是近红外波段,沿轨MTF值在各频率处比跨轨和 45° 方向的MTF值高,而且沿轨MTF从低到高频率衰减的速度比较平缓,尤其是在低频处。红波段沿轨MTF从 $0.1-0.2, 0.2-0.3, 0.3-0.4, 0.4-0.5$ 频率依次衰减速度为 $10.84\%, 13.71\%, 16.01\%$ 和 7.68% ;跨轨和 45° 方向MTF各频率处的衰减速度分别为 $14.59\%, 8.96\%, 14.91\%, -6.08\%$ 和 $29.29\%, 18.62\%, 4.9\%, 6.9\%$ 。近红外波段的这种现象更加明显,0.2频率处MTF值的衰减率将直接影响着波段半带宽的大小。

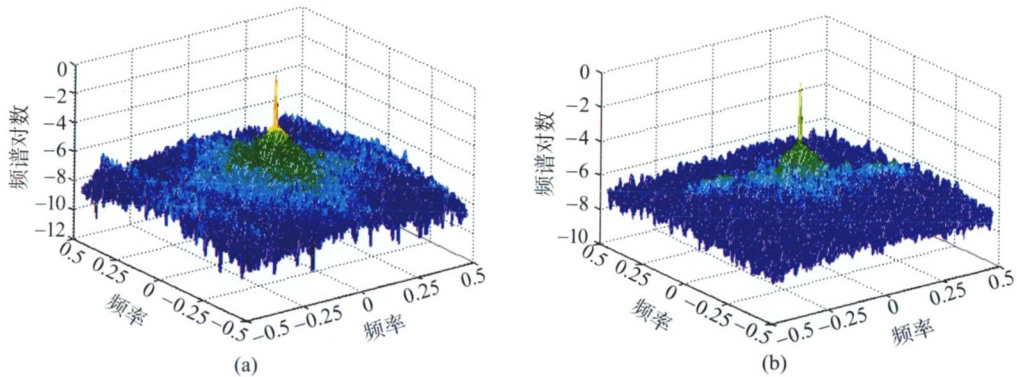


图3 WFI与CCD图像FFT变换后取对数的图像
(a) WFI; (b) CCD

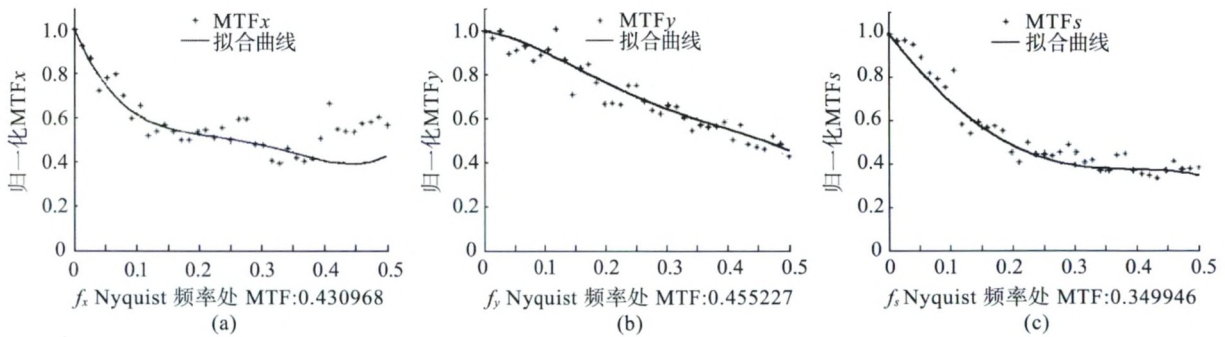


图4 WFI相机红波段3个方向的MTF
(a) 跨轨MTF; (b) 沿轨MTF; (c) 45° 方向MTF

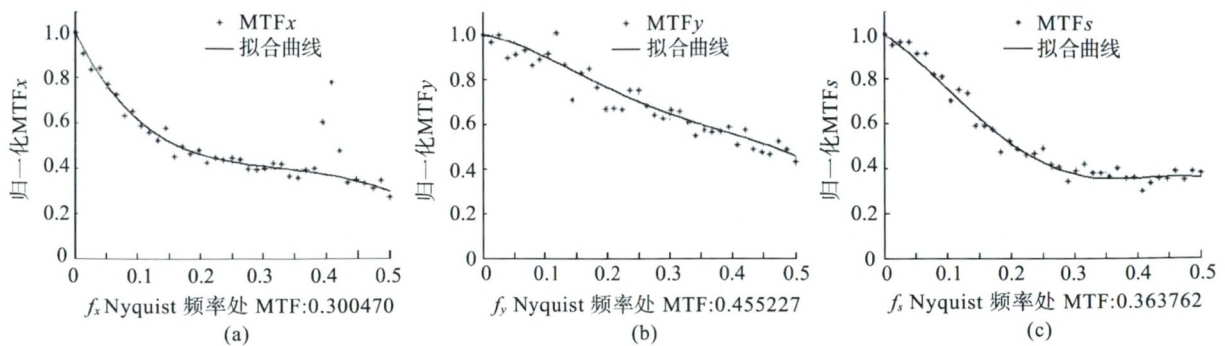


图5 WFI相机近红外波段3个方向的MTF
(a) 跨轨MTF; (b) 沿轨MTF; (c) 45° 方向MTF

利用测得的 MTF 反推出 3 个方向的线扩展函数 LSF, 可算出不同方向的半带宽, 即有效瞬时视场, 如图 6。图中表明, CCD 相机第 3 波段的有效瞬时视场在跨轨方向、沿轨方向及 45° 方向大于 1 个像元, 为 1.188, 1.165 与 1.281 个像元, 即 306.5, 300.5 和 330.5m; 近红外波段为 1.258, 1.195

与 1.326 个像元, 即 324.5, 308.3 和 342.1m。同系列的前一卫星, CBERS-02 的 WFI 红波段 3 个方向有效瞬时视场分别为 1.23, 1.18 及 1.24 个像元。CBERS-02B 卫星的 WFI 与 CBERS-02 卫星的 WFI 相比, 红波段的 MTF 特性在跨轨与沿轨方向有所提高。

表 3 WFI 红波段与近红外波段 3 个方向各频率处的 MTF 值

		0.1 频率	0.2 频率	0.3 频率	0.4 频率	0.5 频率
红波段	跨轨 MTF	0.6141	0.5245	0.4775	0.4063	0.4310
	沿轨 MTF	0.8746	0.7798	0.6729	0.5652	0.5218
	45°方向 MTF	0.6865	0.4854	0.3950	0.3757	0.3499
近红外波段	跨轨 MTF	0.6145	0.4621	0.4127	0.3758	0.3005
	沿轨 MTF	0.9019	0.7639	0.6437	0.5525	0.4552
	45°方向 MTF	0.7549	0.5120	0.3783	0.3602	0.3638

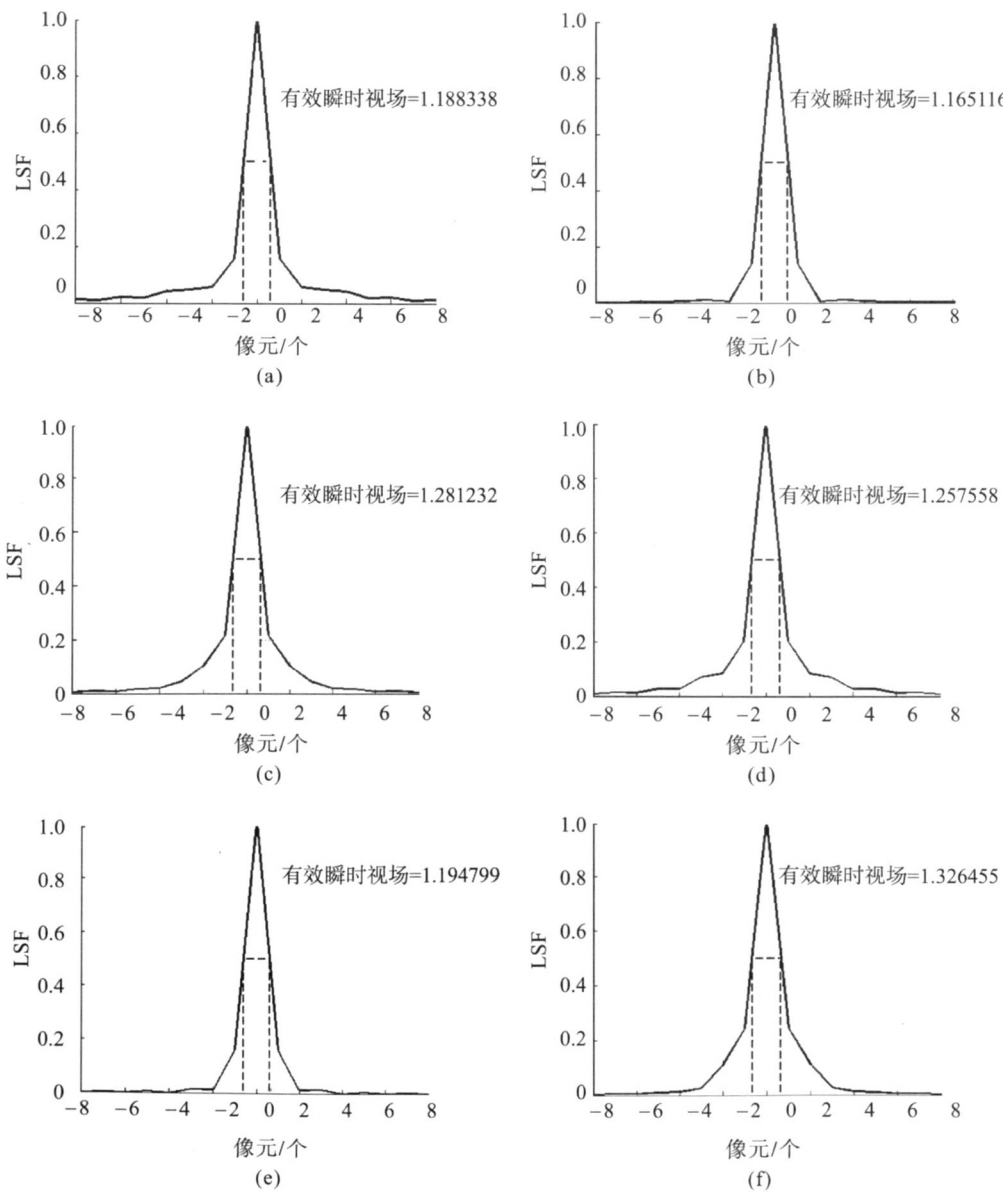


图 6 WFI 相机两个波段 3 个方向的 PSF

- (a) 红波段跨轨 PSF; (b) 红波段沿轨 PSF; (c) 红波段 45°方向 PSF; (d) 近红外波段跨轨 PSF;
- (e) 近红外波段沿轨 PSF; (f) 近红外波段 45°方向 PSF

5 对 WFI 图像的 MTF 补偿

文中基于 CBERS-02B 卫星 WFI 在轨 MTF 测量结果, 对 WFI 图像进行 MTF 补偿。利用 Gu 等, (2005) 和 李小英(2006) 改进的二维 MTF 构建方法, 计算 WFI 的二维 MTF, 用于 MTF 补偿模型。本文选择维纳滤波法模型对 WFI 图像进行 MTF 补偿。

维纳滤波法在图像恢复中是一种很常用的算法 (Fonseca 等, 1993; Li, 2006; Liu 等, 2004), 它可直接用于频率域。频率域的维纳滤波器算子如下式所示:

$$P(u, v) = \frac{1}{\text{MTF}(u, v)} \times \left[\frac{\text{MTF}(u, v)^2}{\text{MTF}(u, v)^2 + k_w} \right] \quad (3)$$

$$R(u, v) = I(u, v) \times P(u, v) \quad (4)$$

式中, $P(u, v)$ 是维纳滤波器, k_w 与图像的信噪比有关, 为信噪比的倒数。一般可以用一个先验的常数来代替; $R(u, v)$ 为恢复图像的频谱, $I(u, v)$ 是原始图像的频谱; $\text{MTF}(u, v)$ 为二维 MTF 矩阵。

图 7 与图 8 分别 2007-11-10 获取的轨道号 1/53 WFI 两个波段进行 MTF 补偿前后的子图像。比较图中 WFI 补偿前后图像, 可以看到 WFI 图像 MTF 补偿后图像的清晰度提高, 细部信息明显。如中间白色指示框中, 这是成格子形状的渤海湾沿海地区水产养殖池或滩涂, 在 WFI 红波段与近红外波段补偿后图像中可见比较清晰的格子状纹理。为了方便比较, 将右上角的白色指示框放大, 框中左上角线状排列地物在补偿后图像上纹理更加明显, 其他不同亮度地物的边缘对比度在 WFI 红波段与近红外波段补偿后图像中也更加清楚。WFI 补偿后图像中的河流比原图像显得线条更加清楚。

虽然 MTF 补偿在很大程度上恢复了图像的细部信息, 改善了原图像中地物边缘模糊的现象。然而 MTF 补偿也会带来一定的问题, 即噪声放大。从图 7 和图 8 中 MTF 补偿前后的放大窗口可以看出原图比较平滑, 而 MTF 补偿后图像上增加了带有纹理或随机的高频噪声。目前, 如何能在 MTF 补偿过程中有效的抑制噪声放大是国际上的一大研究热点, 作者也将进一步研究。

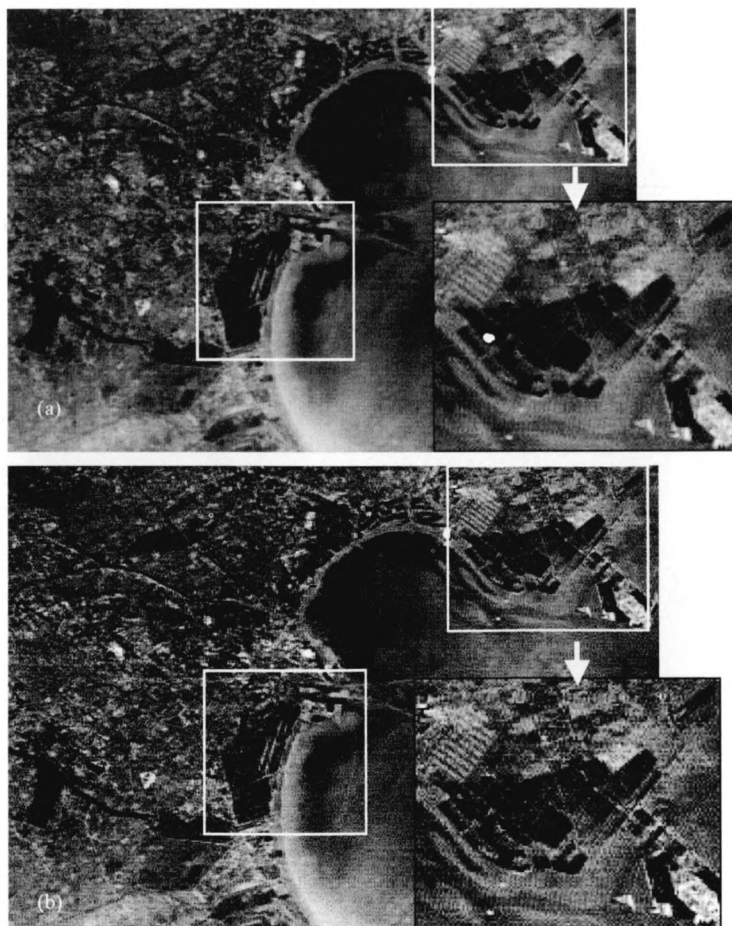


图 7 2007-11-10 1/53 WFI 图像红波段 MTF 补偿

(a) 原始图; (b) 补偿图

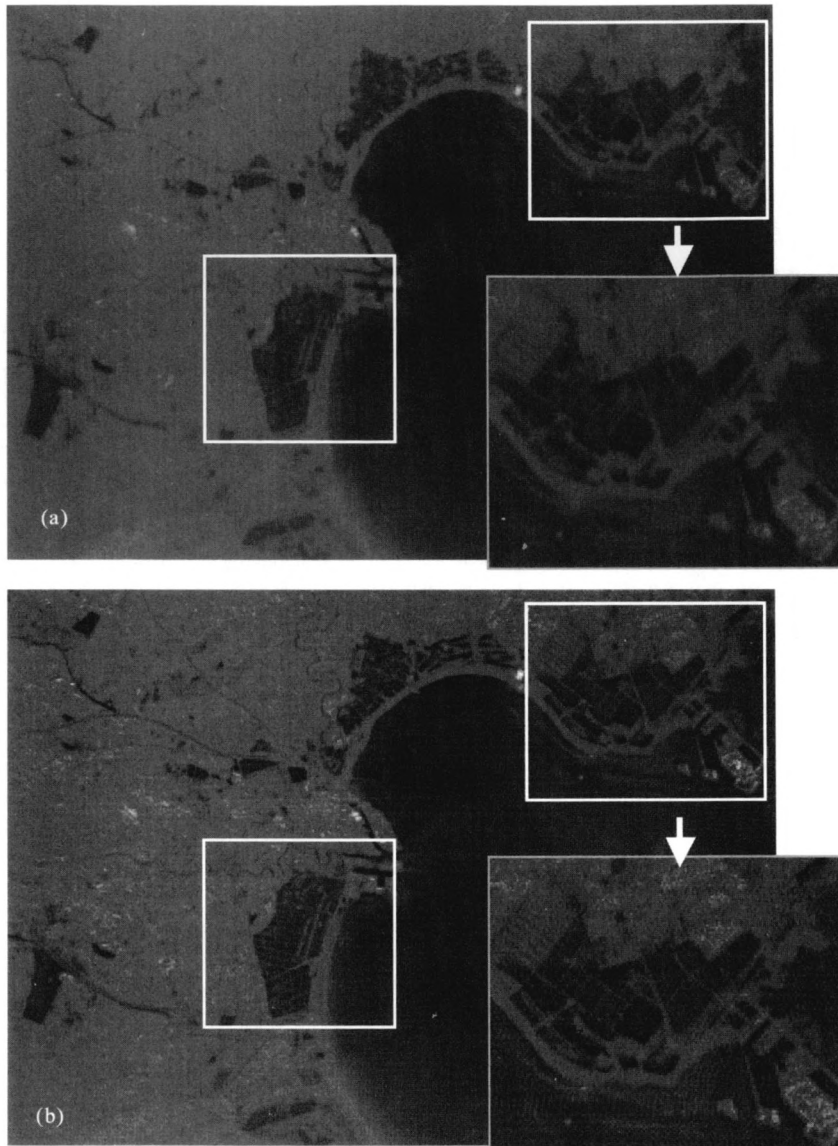


图 8 2007-11-10 1/53 WFI 图像近红外波段 MTF 补偿
(a) 原始图; (b) 补偿图

6 结 论

利用同一平台上的高分辨率图像(CCD 相机图像)评价及测量 WFI 图像的 MTF, 获得了 WFI 图像 3 个方向的 MTF 曲线及半带宽。WFI 相机红波段跨轨、沿轨与 45° 方向有效瞬时视场分别为 1.188, 1.165 与 1.281 个像元; 近红外波段为 1.258, 1.195 与 1.326 个像元。基于在轨测量的 MTF, 对 WFI 图像进行 MTF 补偿以改善图像质量。研究表明, 高分辨率对比法适用于类似 WFI 这种中低空间分辨率传感器的在轨 MTF 测量; MTF 补偿结果表明 MTF 补偿后的图像边缘部分对比度加强, 细部信息更丰富。

由于利用高空间分辨率图像对比法的测量结果与高空间分辨率图像的质量直接相关, 由于这种质

量很难定量给出, 使得结果带有一定不确定性。另外 MTF 测量结果也会因实验场景的不同有不同的结果。因为用于测量 WFI 成像仪在轨 MTF 的图像只有一个时相一个场景, 需要进一步利用更多的像对进行在轨 MTF 测量, 以验证结果与精度分析。另外由于 MTF 补偿过程会带来噪声放大, 使得 WFI 图像补偿后产生了高频噪声, 需要进一步探讨 MTF 补偿模型, 以期较好的在恢复图像信息过程中同时抑制噪声的产生。

致 谢 感谢资源卫星应用中心提供了相关的 CCD 与 WFI 图像。

REFERENCES

Bretschneider T, Bones P J, McNeill S and Pairman D. 2001.

- Image-based quality assessment of SPOT data. Proceedings of the American Society for Photogrammetry & Remote Sensing, St. Louis, April, 2001
- Du H and Voss K J. Effects of point-spread function on calibration and radiometric accuracy of CCD camera. *Applied Optics*, **43** (3): 665—670
- Fonseca L M G, Prasad G S S D and Mascarenhas N D A. 1993. Combined interpolation—restoration of Landsat images through FIR filter design techniques. *International Journal of Remote Sensing*, **14** (13): 2547—2561
- Forster B C and Best P. 1994. Estimation of SPOT P-mode point spread function and derivation of a deconvolution filter. *ISPRS Journal for RS and GIS*, **49** (6): 32—42
- Gu X F, Li X Y, Min X J, Yu T, Sun J J, Zeng Y, Xu H and Guo D. 2005. In flight MTF monitoring and compensation for CCD camera on CBERS-02. *Science in China Series E-Engineering & Materials Science*, **48** (Suppl.1): 29—43
- Kohm K. 2004. Modulation transfer function measurement method and results for the orbview-3 high resolution imaging satellite. Proceedings of ISPRS 2004, Istanbul, Turkey, July 12—23
- Leger D, Viallefont F, Hillairet E and Meygret A. 2003. In-flight refocusing and refocusing and MTF assessment of SPOT5 HRG and HRS. *SPIE*. **4881**: 224—231
- Li X Y. 2006. In Flight Radiometric Calibration and Pixel Based Calibration for CCD Camera and WFI Imager on CBERS-02. Ph.D dissertation of the Institute of Remote Sensing Applications, CAS
- Li X Y, Gu X F and Yu T. 2009. In-flight MTF measurement and compensation for CBERS-02 WFI imager. *International Journal of Remote Sensing*, **30**(4): 829—839
- Liu Z J, Wang C Y and Luo C F. 2004. Estimation of CBERS21 Point Spread Function and Image Restoration. *Journal of Remote Sensing*, **8** (3): 234—238
- Schowengerdt R A, Archwamety C and Wrigley R C. 1985. Landsat thematic mapper image-derived MTF. *Photogrammetric Engineering and Remote Sensing*, **51** (9): 1395—1406
- Taeyoung Choi. 2002. IKONOS Satellite on Orbit Modulation Transfer Function (MTF) Measurement Using Edge and Pulse Method. A thesis Submitted in Partial Fulfillment of the Requirements for the Master of Science Major in Engineering South Dakota State University
- Viallefont-Robinet F and Henry P. 2000. VEGETATION MTF in-flight measurement using HRVIR. Proceeding of the SPIE-Earth Observing Systems V, **4135**: 314—323

附中文参考文献

- 李小英. 2006. CBERS-02 卫星 CCD 相机与 WFI 成像仪在轨辐射定标与像元级辐射定标研究. 中国科学院遥感应用研究所博士论文
- 刘正军, 王长耀, 骆成凤. 2004. CBERS-1 PSF 估计与图像复原. *遥感学报*, **8**(3): 234—238